8

Robotic Application of IPMC Actuators with Redoping Capability

M. Yamakita[1, 2], N. Kamamichi[2], Z. W. Luo[3, 2], K. Asaka[4, 2]

[1] Department of Mechanical and Control Engineering, Tokyo Institute of Technology
2-12-1 Oh-okayama, Meguro-ku, Tokyo, 152-8552, Japan
yamakita@ctrl.titech.ac.jp
[2] Bio-Mimetic Control Research Center, RIKEN
2271-130 Anagahora, Shimoshidami, Moriyama-ku, Nagoya, 463-0003, Japan
nkama@bmc.riken.jp
[3] Department of Computer and Systems Engineering, Kobe University
1-1 Rokkodai, Nada, Kobe, 657-8501, Japan
luo@gold.kobe-u.ac.jp
[4] Research Institute for Cell Engineering, AIST
1-8-31 Midorigaoka, Ikeda, Osaka, 563-8577, Japan
asaka-kinji@aist.go.jp

8.1 Introduction

Machines and robots have big impacts on our life and industry to realize high-speed, high-power, and high-precision motion; however, recently other factors are demanded, *e.g.*, miniaturization or flexibility. For robots working in ordinary human life, it is desired to use safe and soft actuators, which are sometimes called artificial muscle. A high polymer gel actuator is one of the candidates for artificial muscle actuators due to their softness and miniaturizability.

For several decades, electroactive polymers (EAP) 0, which respond to electric stimuli with shape change, received little attention because of their actuating limitations. During the last ten years, development of EAP materials with large displacement and quick response changed the potential capability, and EAP received much attention from engineers and researchers in many disciplines, *e.g.*, robotics, medical service, and the toy industry.

The ionic polymer-metal composite (IPMC) is one of the most promising EAP actuators for applications. IPMC is produced by chemically plating gold or platinum on a perfluorosulfonic acid membrane which is known as an ion-exchange membrane. When an input voltage is applied to the metal layers of both surfaces, they bend at high speed. The phenomenon of this motion was discovered by Oguro *et al.* in 1992 0. The characteristics of an IPMC are as follows:

Driving voltage is low (1~2 V).
Speed of response is fast (> 100 Hz).

It is durable and stable chemically. (It is possible to bend more than 10^6 times.)
It is a flexible material.
It moves in water and in wet conditions.
Miniaturization and weight saving is possible.
It is silent.
It can be used as a sensor.

By exploiting the characteristics, IPMC actuators have been applied to robotic applications such as an active catheter [3,4], a fish-type underwater robot [4~10], a wiper for a nanorover 0, a micropump 0, a micromanipulator 0, and a distributed actuation device 0.

It, however, also has disadvantages that the actuation force is still small and that the input voltage is restricted to the range where electrolysis of the ionic polymer does not occur. To improve performance, development of the ionic polymer membrane and plating method are required.

IPMC actuators also have another noteworthy property; the characteristics of bending motion depend highly on counterions. In application to mechanical systems such as robots, the possibilities exist to change the properties of the dynamics adequately according to the environment or purpose. We have called this property the “doping effect”, and verified the effect on robotic applications.

The goal of our study is applying an artificial muscle actuator to robotic applications especially to a bipedal walking robot, and we developed a linear actuator using IPMC. The structure of our proposed actuator is very simple, and the actuator transforms bending motion into linear motion. We assume that elementary units are connected in parallel and series to realize the desired displacement and force. In this paper, we describe the structure of the actuator and identify an empirical model of the actuator. Numerical simulations of bipedal walking are demonstrated, and the doping effect is investigated by the walking simulation and an experiment using a snakelike robot. Finally, control of doping speed by exercise is also considered.

8.2 Proposed IPMC Linear Actuator

In this section, the structure and basic properties of the proposed IPMC linear actuator will be explained 0.

8.2.1 Structure of IPMC Linear Actuator

The proposed linear actuator is composed of many basic units connected in parallel and series so that enough force and displacement can be obtained. The structure of the elementary unit is shown in Figure 8.1. This elementary unit consists of four IPMC films. One side of the unit is formed from a pair of films that are connected by a flexible material or the same thin film. When an input voltage is applied to electrodes on the surface with the anode outside, each membrane bends outside, then the actuator is constricted. The actuation force and displacement of each unit

are small; however, the elementary units can be connected in parallel and series as in Figure 8.2, so the actuator can realize the desired force and displacement. By shifting the series of elementary units by a half pitch to avoid interference as in Figure 8.2, the total actuator is made compact, and high power/volume and miniaturization are realized.

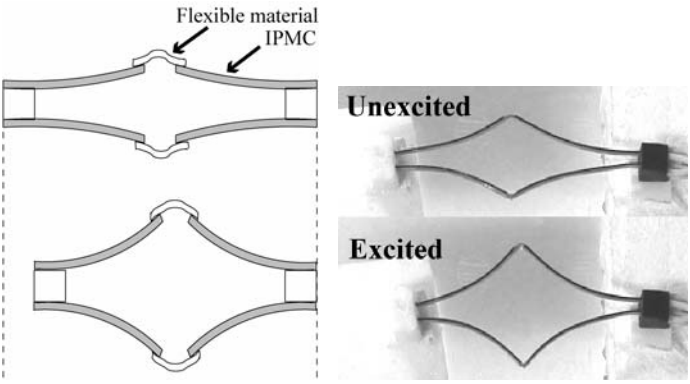

Figure 8.1. Structure of IPMC actuator

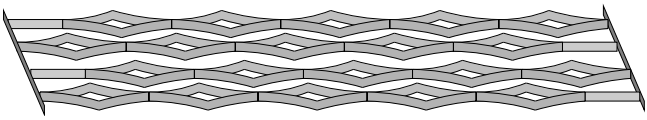

Figure 8.2. Basic concept of IPMC linear actuator

8.2.2 Properties of the Elementary Unit

To check the characteristics of the actuator, we carried out fundamental experiments. Figure 8.3 shows the experimental setup. In this experiment, one edge of the actuator is fixed on a board floating on water to reduce the effects of the weight of electrodes and ties. Displacement of the linear actuator was measured by a laser displacement meter.

8.2.2.1 Response in Step Voltage

Figure 8.4 shows the response in a step voltage without loads, where step input voltages of 1.5, 2.0, and 2.5 V were applied at 0 s. The IPMC film which we used in this experiment is Nafion®117 (DuPont) plated with gold. A counterion doped in the film is Na^+. Though the response of the actuator varies depending on its condition, it was confirmed that the unit whose total length is 40 mm is constricted by 10 mm with a step input voltage of 2.5 V in average. As the applied voltage is increased, the peak value of the displacement is also increased.

In this experiment, it is observed that when a step voltage is applied, the IPMC membrane bends toward the anode side quickly and bends back gradually. The characteristic varies according to the counterion, as mentioned below. It was also

observed that the current increased sharply at the moment when the input voltage was applied, and then it decreased exponentially.

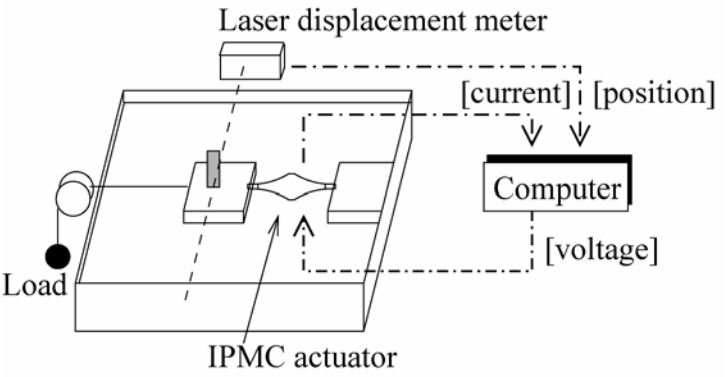

Figure 8.3. Experimental setup

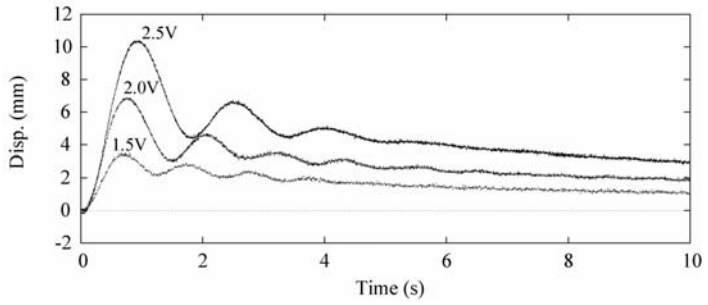

(a)

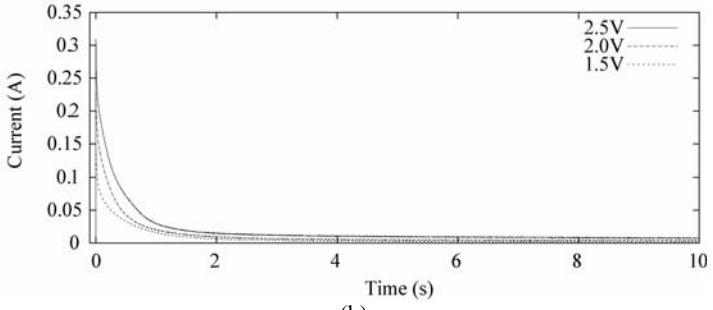

(b)

Figure 8.4. Step response with various inputs (a) displacement (b) current

8.2.2.2 Response with Loads

Figure 8.5 shows the response in step voltage with loads; a step input voltage of 2.5 V was applied in loading. As the load is increased, displacement becomes small but the current almost does not change.

Note that to avoid damage of IPMC actuators by electrolysis, the control input voltage is limited to about 3.0 V. So it is not so effective to change the dynamic properties by changing the control voltage. In the following, changing the dynamic properties chemically is considered by changing the doped ions in the film.

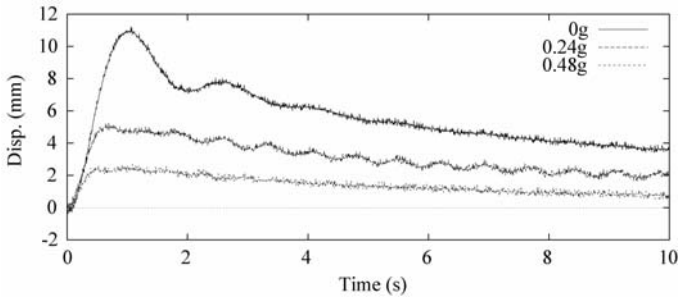

(a)

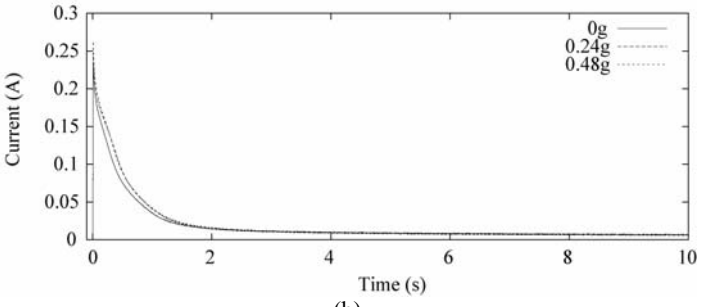

(b)

Figure 8.5. Step response with various loads (a) displacement (b) current

8.2.2.3 Responses with Different Doped Counterions

It is known that IPMC changes bending characteristics with respect to doped counterions 0. Figure 8.6 shows the responses of actuators for the same input voltage of 2.5 V, which are doped with sodium (Na^+), cesium (Cs^+), and tetraethylammonium (TEA^+) as the counterion, respectively. From the figure, it is observed that the raising time of the unit with Na^+ is shorter than that with Cs^+ and the rising time of the unit with TEA^+ is largest. On the other hand, the tendency of the response to decay is large for the unit with Na^+ or Cs^+, but it is very small for the unit with TEA^+. The doping of the counterion is easily done by just putting the unit in a solution containing the target counterion, and higher condensed counterions are doped into IPMC films. Also, the change of the doped ion is reversible. The property suggests that the characteristics of the actuator can be changed for specific purposes. In Section 8.4.3, we will show the effect of doping

in the walking pattern and efficiency of a small bipedal robot, and in Section 8.5 we will show experimental results of doping on a snakelike robot. In 0, it was discussed how to change equivalent characteristics of the actuator mechanically.

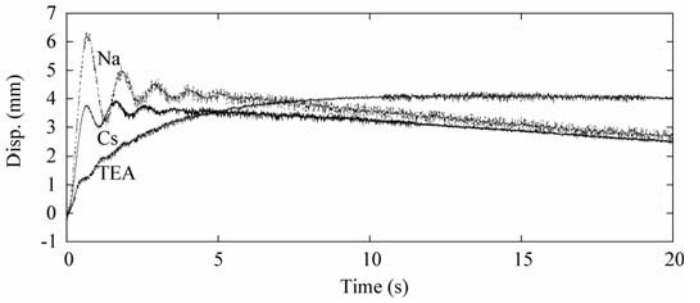

(a)

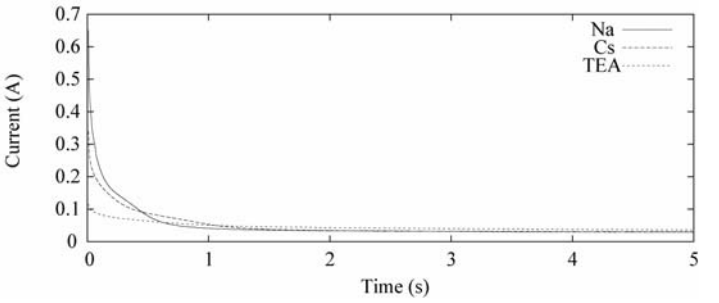

(b)

Figure 8.6. Response with various counterions (a) displacement (b) current

8.3 Model Identification

To know the capability of the linear actuator for a robotic system, we identify the linear actuator as a mathematical model. IPMC actuators have been modeled in various ways as a black or gray box model 0, and a detailed model based the physical and chemical phenomena [19~21]; however, it is difficult to represent these models by systems of ordinary differential equations because of their complexity. In this paper, in consideration of model-based control, we use a gray box model which has two inputs, *i.e.*, control voltage and external force. We identify the actuator as a linear time-invariant model with static nonlinearity from input-output data using a subspace identification algorithm [15,22].

8.3.1 Identification Method

First, the model of the actuator is assumed to be represented by the system in Figure 8.7. This model has two inputs and one output, and it consists of two

subsystems, $P_1(s)$ and $P_2(s)$, which are connected in series. $P_1(s)$ is a system with one input v, input voltage, and one output f_1 which is a force generated by electric stimuli. $P_2(s)$ is a system with one input force f_2 which is exerted on the actuator, and one output y, displacement of actuator. f_2 is assumed to be the difference between f_1 and f_l. $P(s)$ is defined as $P_2(s)\,P_1(s)$.

For the moment, it is assumed that the actuator is driven in a small operating range, and the dynamics is identified as an LTI model as follows:

Identification of $P(s)$: Measure a response from input voltage v to displacement y; then compute the system $P(s)=P_2(s)P_1(s)$ from input-output data using a subspace identification algorithm.

Identification of $P_2(s)$: Measure a response from load f_l to displacement y; then compute the system $P_2(s)$ from input-output data using a subspace identification algorithm.

Computation of $P_1(s)$: Compute the system $P_1(s)$ as $P_2(s)^{-1}P(s)$.

In procedures 1 and 2, we performed the system identification using the N4SID function in MATLAB, and from the discrete time model obtained, the corresponding continuous model was determined.

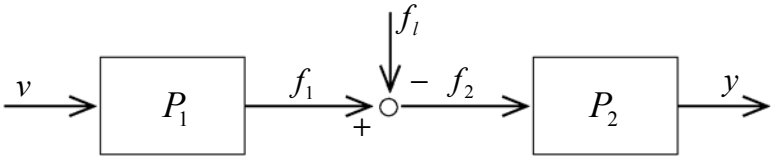

Figure 8.7. Block diagram

8.3.2 Identification Results

We obtained estimated transfer functions of the systems as

$$P_1(s) = -\frac{1.50\times10^{-3}s^2 + 1.09\times10^{-2}s + 3.93\times10^{-2}}{s^3 + 6.13s^2 + 3.23\times10s + 7.12\times10} \tag{8.1}$$

$$P_2(s) = -\frac{3.49\times10^{3}s^2 + 1.23\times10^{6}s + 3.81\times10^{6}}{s^4 + 7.19s^3 + 6.49\times10^{4}s^2 + 4.14\times10^{5}s + 1.33\times10^{6}}$$

If the relative degree of $P_2(s)$ is 2, then it is easy to simulate an impulsive effect of collision. In procedure 2, the relative degree of $P_2(s)$ was estimated as 1, but the coefficient of the highest order term in the numerator of $P_2(s)$ was much smaller than the other. Thus we eliminated it, and obtained the transfer function whose relative degree is 2. In procedure 3, small coefficients of $P_1(s)$ ware also eliminated.

Figure 8.8 shows a comparison between the experimental result and the simulation result using the identification model. It is shown that a quick transient of simulation result is nearly equal to the experimental one. But in part of the slow decay, there is a little error between them. As the results of identification with a linear approximate model, the characteristics of the actuator are captured.

When the control voltage and external load are given simultaneously, as in Figure 8.9, we can observe the large error between them. The reason for the error can be inferred as nonlinear effects due to the large deformation of the structure of the unit. So we should consider other models to deal with such a large deformation and the nonlinearity.

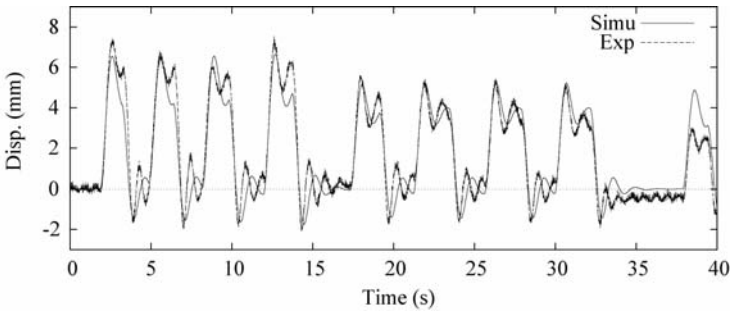

Figure 8.8. Identification result 1

8.3.3 Introduction of Nonlinear Effect

To reduce the error due to nonlinearity, a nonlinear compensation term is introduced. First, the system is identified as an LTI model and static nonlinearity which is represented as a polynomial or weighted sum of Gaussian functions is introduced, *i.e.*, we use a Hammerstein model for the P_2 part. Weights for the basis functions are determined to minimize the mean square error. Figure 8.9(b) shows the result with the nonlinear terms. To the inputs of $P_2(s)$, f_1 and f_l, nonlinear elements which are represented as a weighted sum of Gaussian functions and polynomials are introduced. Compared to the result of Figure 8.9 (a), it can be seen that the mean square error is reduced by 40% and the model is valid for a large operating range.

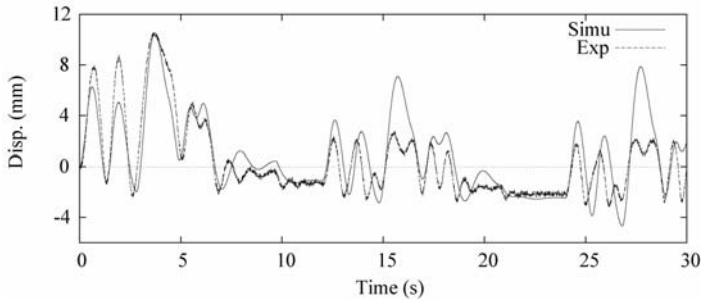

(a)

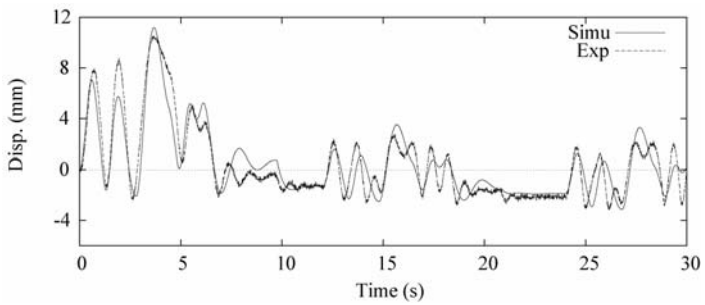

(b)

Figure 8.9. Identification result 2 (a) LTI identification (b) identification with nonlinear terms

8.3.4 Experiment of Feedback Control

To check the validity of the identified model, a feedback control experiment using an LQ servocontroller was conducted.

A position controller was designed based on the Hammerstein model and an LQ servocontroller was designed for a compensated Hammerstein model. Because the Hammerstein model contains static nonlinearity in front of the LTI part, the nonlinearity is compensated by the inverse system of the nonlinear function, and a linear controller was designed for the LTI part. Figure 8.10 shows a whole system composed of the Hammerstein model and the designed controller. The controller is designed as follows:

(1) Design a linear controller K for LTI part P,

(2) Put $N^{-1}K$ in front of the Hammerstein model $P\,N$.

Please notice that in general the nonlinear block N might not be invertible. There, however, exists N^{-1} for our model during the considered operating range.

Figure 8.11 shows the control results. The state of the system required for an LQ servecontroller was estimated by a linear observer. The actuator used for the experiment was composed of IPMC films doped with Na^{+}. From the figure, it is

observed that the desired position control is achieved, though some oscillation is observed. In figure (b), the control voltage of the experiment and simulation are shown and we can see some deviation. Especially, the actual control voltage gradually increased due to integral operation. The reason inferred for the deviation is that such a slow mode was not identified by our Hammerstein model. We consider, however, that our model is valid for a periodic motion with a short period considered below.

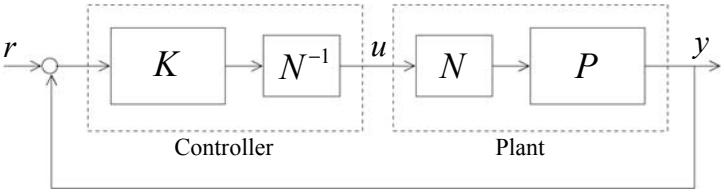

Figure 8.10. Design of controller

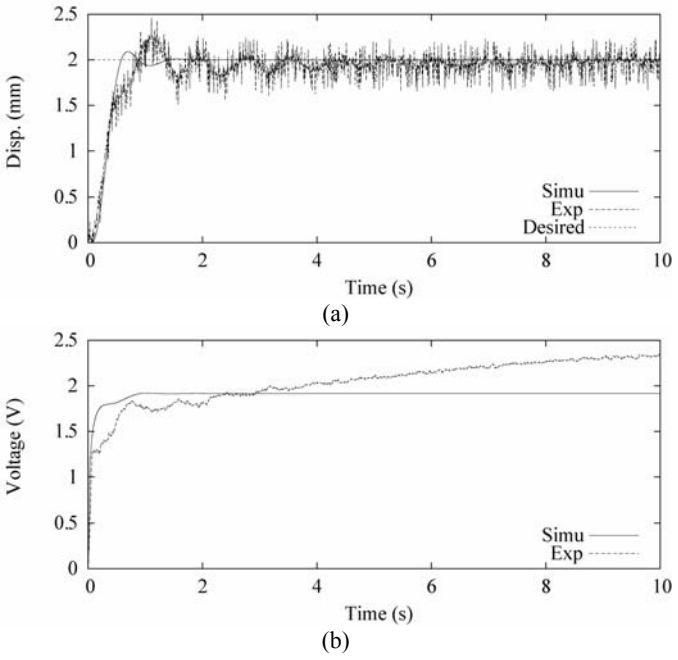

Figure 8.11. Experimental result of position control (a) displacement (b) input voltage

8.4 Application to Walking Robot

This section addresses an application of the linear actuator to a small-sized bipedal walking robot shown in Figure 8.12, and realization of walking with the proposed actuator is investigated by numerical simulations. The parameters of the robot are set as m_l=5 g, m_h=10 g, a=50 mm, b=50 mm, l=100 mm, r_h=4 mm, g=9.81 m/s^2, and r_f=0 mm. This small bipedal robot can exhibit passive dynamic walking 0 without any actuator on a gentle slope. In the following simulation, we assume that actuators are attached between legs, as in the right side of Figure 8.12. In the simulations, we assume that contact between a leg and ground is pin contact and collision of the swing leg with the ground is perfectly inelastic.

8.4.1 Simulation Results

Figure 8.13 shows the simulation results of walking on level ground. The number of units connected in parallel and series is set as 4 and 3, respectively. In this simulation, we applied a square pulse as input voltage whose cycle was 0.48 s and whose amplitude was 2.5 V. From the results, it can be seen that a one-period walking gait is generated and the walking cycle synchronizes with the cycle of the input signal.

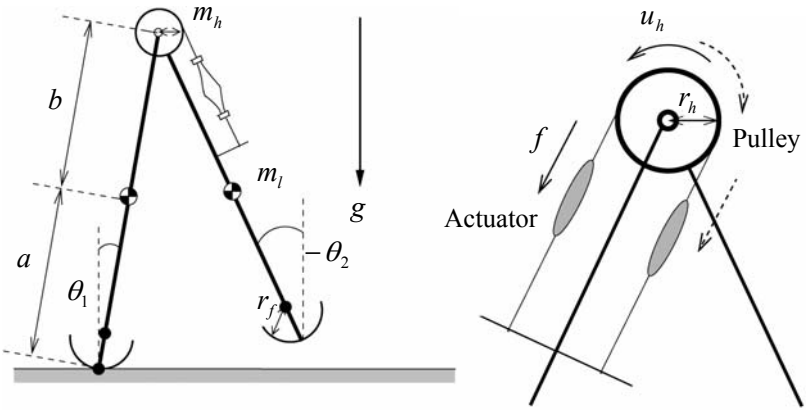

Figure 8.12. Model of bipedal walking robot

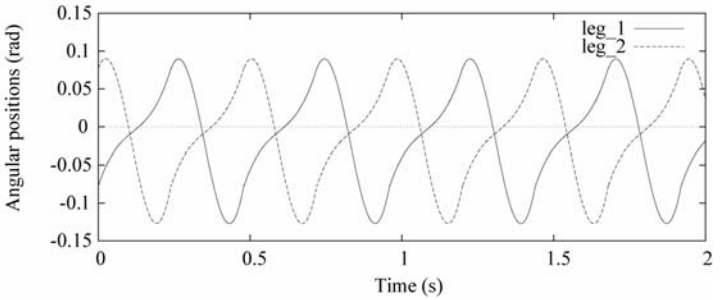

(a)

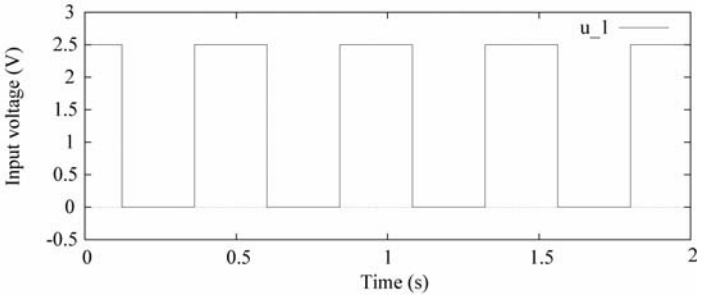

(b)

Figure 8.13. Simulation results of walking on level ground (a) angular positions (b) input voltage

8.4.2 Walking Control with Synchronization

8.4.2.1 Open-Loop Control

In the previous section, we applied time-variant signals as open-loop inputs, *i.e.*, constant periodic square pulses, and it was shown that the bipedal walking robot with actuators can walk on level ground with the period synchronized with the period of the input signal. In this section, we consider time-invariant input signals, that is, switch the input signals in response to the state of the robot, *e.g.*, the angle of a stance leg.

Figure 8.14 shows the simulation results of open-loop control. In this simulation, the parameters of the robot are set as m_l= 9.6 g, m_h =32.1 g, a=42.9 mm, b=56.9 mm, l=99.8 mm, r_h =11.3 mm, g=9.81 m/s^2, and r_f=0 mm due to an experimental system, and the input signals are switched by the angle of a stance leg. From the results, it is observed that a one-period walking gait is generated. In comparison with time-variant input, there is not much difference in the convergence to steady state or the basin of attraction; however, we are able to simplify the experimental setup and to adjust easily the timing of inputs and the start of walking. Moreover, the systems with the open-loop inputs are autonomous, then we can apply a simple feedback control method, as described below.

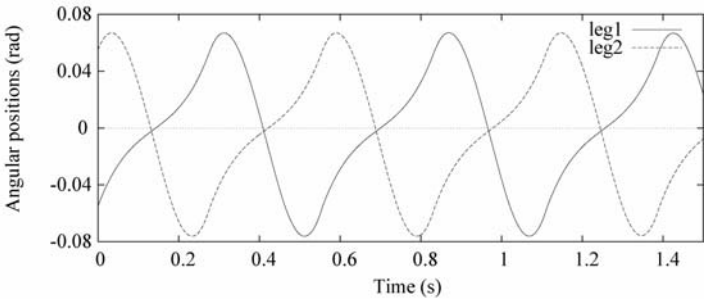

(a)

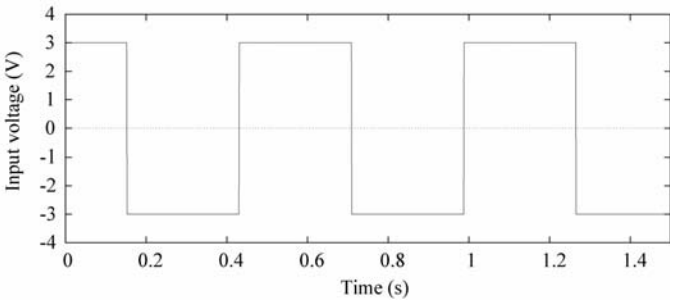

(b)

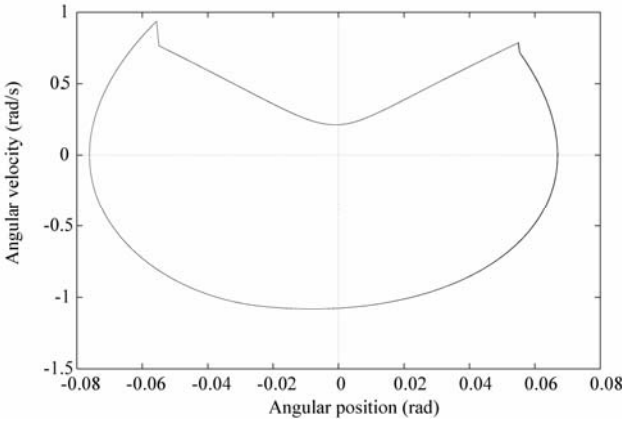

(c)

Figure 8.14. Simulation results of open-loop control (a) angular positions (b) input voltage (c) phase plane

8.4.2.2 Feedback Control

Robots with the actuator can walk on level ground with open-loop control; however, the walking gait is not robust, and the basin of attraction of the limit cycle is limited; then it is difficult to continue walking under the disturbance. To realize robust walking and to enhance the basin of attraction, we apply a feedback control based on the linear approximate model of trajectories on a limit cycle 0.

Figure 8.15 shows a conceptual diagram of trajectories. γ is a periodic orbit through the point q_0, and Σ is a hyperplane perpendicular to γ at q_0; then for any point $q \in \Sigma$ sufficiently near q_0, the orbit will cross Σ again at a point $P(q)$; Σ is called a Poincaré section. It is considered a discrete time nonlinear system on Σ, called a Poincaré map, as follows:

$$q_{k+1} = P(q_k, u_k) \tag{8.2}$$

q^*, u^* are the equilibrium state and input where the equation $q^*=P(q^*, u^*)$ holds. Let $\delta q_k, \delta u_k$ be small perturbations from the equilibrium state and input, *i.e.*, $\delta q_k = q_k - q^*, \delta u_k = u_k - u^*$. Linearizing Eq. (8.2) around q^* and u^* results in the linear system

$$\begin{aligned} \delta q_{k+1} &= \left.\frac{\partial P}{\partial q}\right|_{\substack{q=q^* \\ u=u^*}} \delta q_k + \left.\frac{\partial P}{\partial u}\right|_{\substack{q=q^* \\ u=u^*}} \delta u_k \\ &= \Phi \delta q_k + \Gamma \delta u_k \end{aligned} \tag{8.3}$$

Assume the cycle is stable and the pair (Φ, Γ) is controllable. To stabilize the walking motion and enhance a basin of attraction, we consider the regulator problem based on the discrete time linear system of Eq. (8.3). In this paper, a performance index is defined as

$$J := \sum_{k=0}^{\infty} (\delta q_k^T Q \delta q_k + r \delta u_k^2) \tag{8.4}$$

and we solve the LQR optimal control problem to determine a feedback control input $\delta u_k = F \delta x_k$ where F is an optimal feedback gain matrix determined from J.

8.4.2.3 Numerical Simulation

We demonstrate numerical simulations, and the parameters of the robot are the same as in the previous simulation. In this simulation, we define the Poincaré section Σ in the state just after the heel strike collision, and the state vector q_k is defined as $q_k = [q_{1k,}\ q_{2k,}\ q_{3k}]^T$, where q_{1k} is the angle of the hip joint, q_{2k} is the angular velocity of the stance leg, and q_{3k}, is the angular velocity of the swing leg.

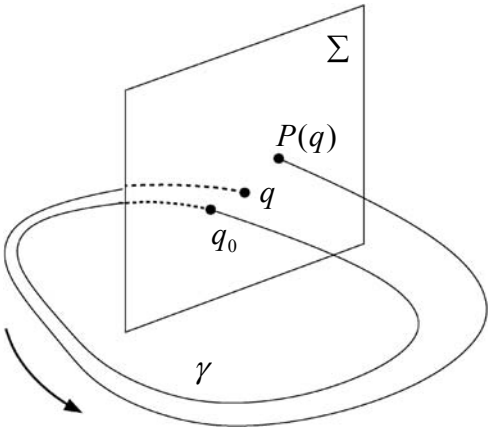

Figure 8.15. Poincaré map

Because Φ, Γ can not be obtained analytically, we computed them numerically by computer simulation as

$$\Phi = \begin{bmatrix} 2.82\times10^{0} & -3.94\times10^{-1} & 3.73\times10^{-2} \\ 1.30\times10^{1} & -1.59\times10^{0} & 1.55\times10^{-1} \\ -1.44\times10^{0} & 7.10\times10^{-1} & -2.29\times10^{-2} \end{bmatrix} \tag{8.5}$$

$$\Gamma = \begin{bmatrix} 9.25\times10^{-3} \\ 5.42\times10^{-2} \\ 4.26\times10^{-2} \end{bmatrix} \tag{8.6}$$

The weighting matrices Q, r are determined as follows:

1. Check the limit of stability; let q_{1f}, q_{2f}, q_{3f} be the quantity of state in the stability limit, respectively, and check them by numerical simulation, that is, we search the maximum perturbation that the robot does not even fall down.

2. Determine Q; Q is set as $Q = \mathrm{diag}(1/q_{1f}^2, 1/q_{2f}^2, 1/q_{3f}^2)$.

3. Determine r; r is adjusted manually to obtain a suitable input.

Figure 8.16 shows the simulation results of feedback control; deviations are included in initial conditions. Q, r, and feedback vector F are

$Q = \mathrm{diag}(3.42\times10^{5}, 9.61\times10^{3}, 8.73\times10^{1})$

$r = 1.0$

$F = [7.76\times10^{1}, -1.02\times10^{2}, 9.80\times10^{-1}]$

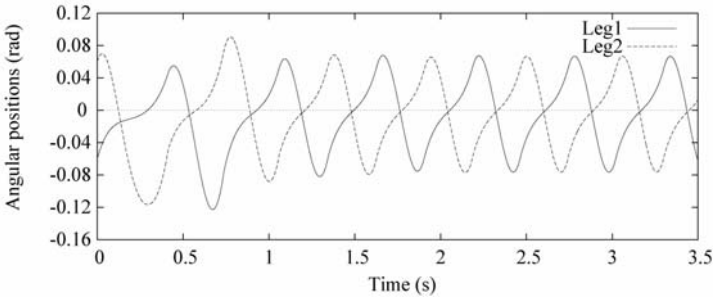

(a)

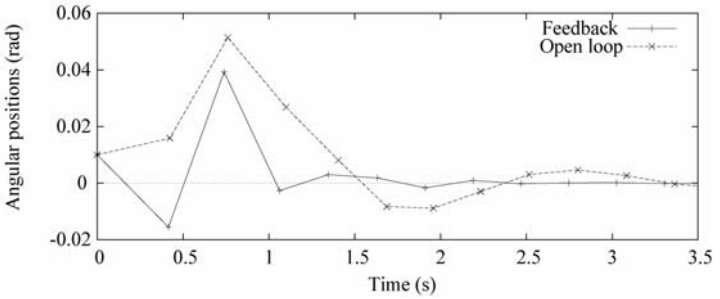

(b)

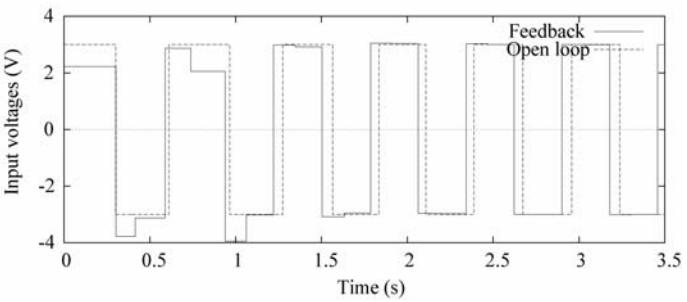

(c)

Figure 8.16. Simulation results of feedback control (a) angular positions (b) transition of δq_1 (c) input voltage

Figure 8.16(a) shows angular positions, figure (b) shows the transition of δq_1 on Poincaré section Σ, and figure (c) shows the input voltage to the actuator, the total of the open-loop signal and feedback signal. From the results, it is observed that the convergence to steady state becomes fast in comparison to open-loop control. The validity of this feedback control was investigated, but more detailed analysis of the basin of attraction and the robustness of the control is left for future work.

8.4.3 Doping Effect on Walking

As shown in the previous section, the bending characteristics of IPMC film are highly affected by the doped counterion. There exist possibilities to change the properties of the actuator according to the environment or purpose. If we consider walking application, we can change the property so that the actuator is suitable for slow walking with low energy consumption or fast walking with high energy consumption, or possibly running. We investigate the possibility of adaptation with doping of the actuator for walking control by numerical simulations 0. Recall that the doped ion can be exchanged as many times as required.

We compare walking speeds and walking efficiencies with actuators composed of IPMC films doped with Na^+ and Cs^+ for the same input voltage. The input voltage is rectangular, its amplitude is 2.5 V, and it is applied to the system in an open-loop fashion. The parameters of the robot are set as m_f=5.0 g, m_h=10.0 g, a=50.0 mm, b=50.0 mm, l=100.0 mm, r_h=4.0 mm, r_f = 0.0 mm, and g=9.81 m/s^2. We assume also that in the simulation the number of units connected in parallel and series is set as 4 and 3, respectively.

Figure 8.17(a) shows a plot of average walking speed vs. the applied frequency of the input where the solid line shows the plot for the actuator with Na^+ and dotted line for that with Cs^+. From the figure, it can be seen that if the same control frequency input is applied to the robot, faster walking is realized by the actuator doped with Na^+ rather than by that with Cs^+. The maximum speed of the robot doped with Na^+ is higher than that with Cs^+. Note here that this kind of property may not exist if the parameters of the robot are not designed properly. So the design of the robot is important for the doping to be effective for walking. Figure 8.17(b) shows a plot of walking speed vs. the average consumed power. Because the input current for the actuator is almost irrelevant to the walking pattern, the peak value of the injected current of the actuator doped with Na^+ is large, and the corresponding consumed power is large.

From the observation, it can be suggested that if the input voltage is the same, the actuator doped with Na^+ realizes high-speed walking with high energy consumption, and the one doped with Cs^+ can generate a slow walking pattern with low energy consumption when the mass is rather heavy, *i.e.*, m=5 g. On the other hand, when m=1 g, the actuator with Cs^+ can realize a wide range of walking speeds with low energy consumption. Note here that even if the average input power is increased in the case of Cs^+, the walking speed is not increased because the walking pattern is not proper and the energy dissipated in a collision is increased.

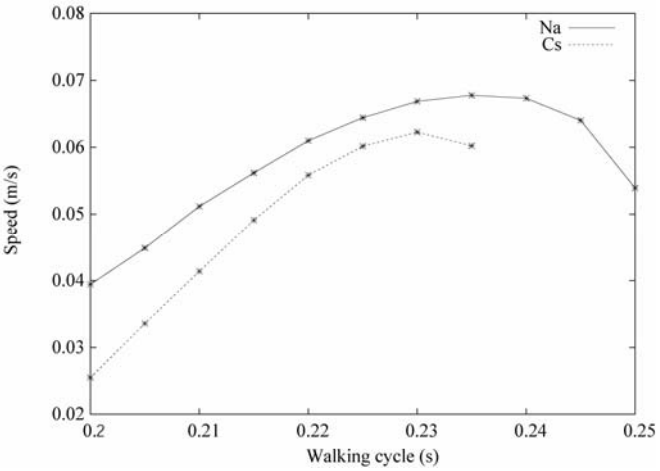

(a)

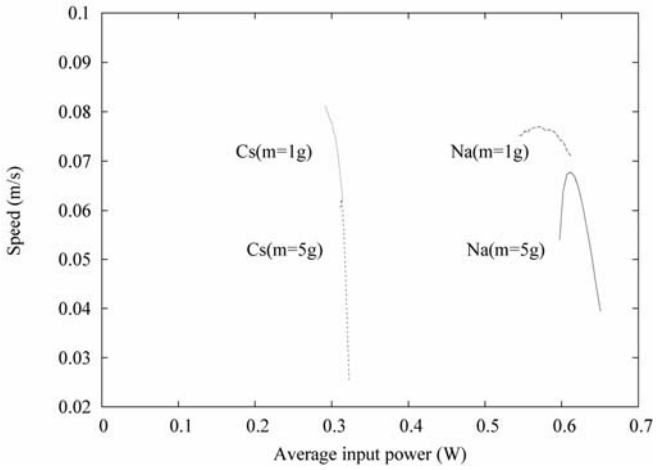

(b)

Figure 8.17. Simulation results of the doping effect on bipedal walking (a) average speed vs. walking cycle (b) average speed vs. average input power

8.5 Application to Snakelike Robot

In the last section, it was shown that the efficiency of walking with different walking speeds was confirmed by numerical simulation. In this section, the effect is checked by a snakelike robot swimming in water experimentally.

8.5.1 Snakelike Robot

Figure 8.18 shows an experimental machine, a three-link snakelike swimming robot with IPMC actuators. The frame of the robot is made of styrene foam. Thin fins are attached to the bottom of the body frame, and each frame is connected by an IPMC film. The total mass of the robot is 0.6 g and its total length is 120 mm. The IPMC film which we used in this experiment is Nafion®117 (by DuPont) plated with gold; the thickness of this film is about 200 μm in a wet condition, and it was cut into a ribbon with a width of 2 mm and length of 20 mm.

To check the performance of the robot, we also performed experiments using the snakelike robot as shown in Figure 8.18.

Figure 8.19 shows the experimental results with input signals whose cycle is 2 s, amplitude is 2.5 V, phase shift is 90°, and the kind of counterion is sodium (Na^+). From figures (a) and (b), it can be confirmed that the robot performs an undulating motion and moves forward. Figure 8.20 shows sequential photographs of the experiment. For more details of the experimental setup and the properties of the motions, refer to 0.

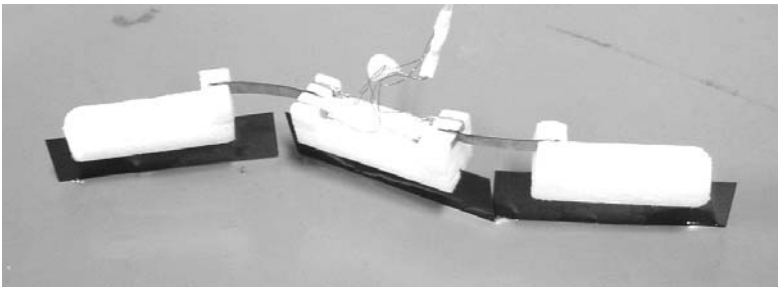

Figure 8.18. Snakelike robot using IPMC

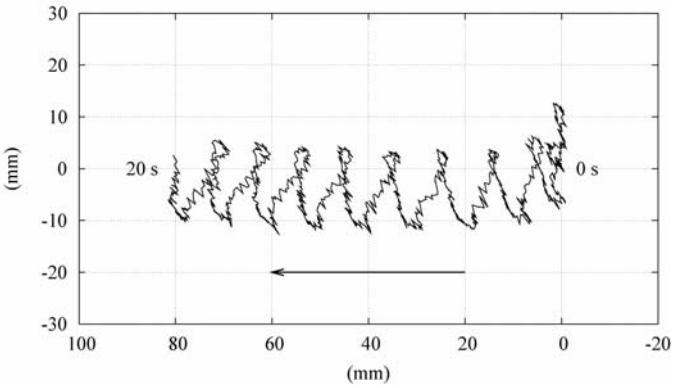

(a)

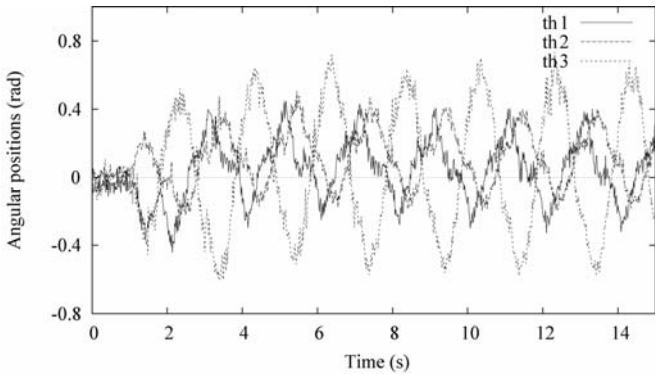

(b)

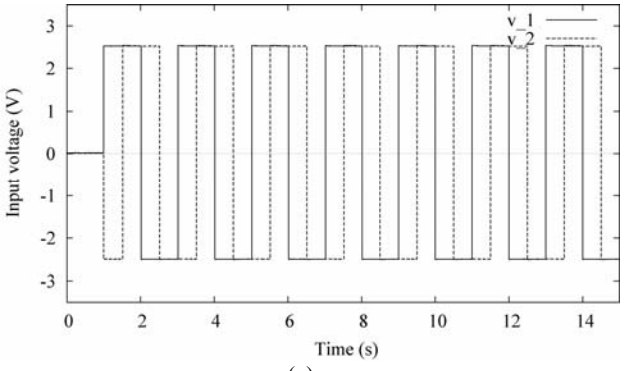

(c)

Figure 8.19. Experimental results (a) trajectory of head position (b) angular positions (c) input voltages

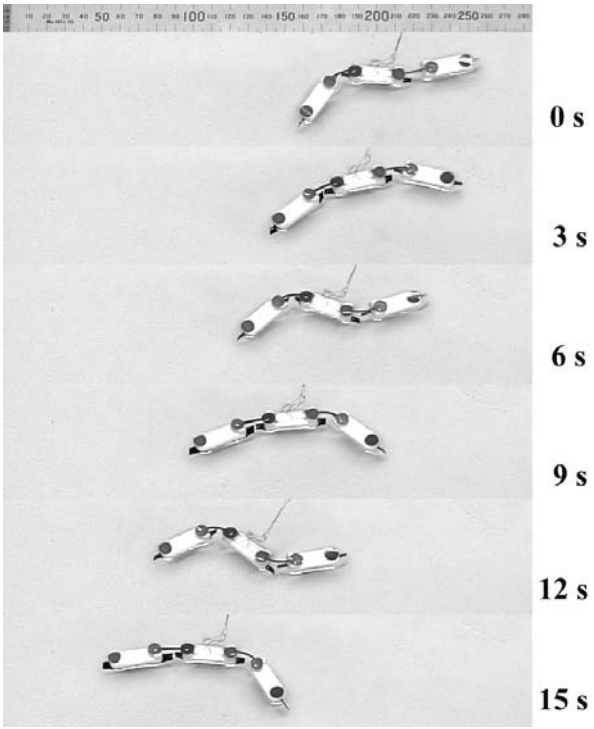

Figure 8.20. Sequencial photographs of the experiment

8.5.2 Doping Effect

To verify the doping effect, we performed experiments on IPMC actuators which were doped with Na^+, Cs^+ and TEA^+ as counterions. We compare propulsive speed and efficiencies of the actuators doped with each ion for the same input voltage. The inputs voltages were square pulses whose amplitude was 2.5 V and phase shift was 90°, and we repeated measurements at various input frequencies.

In Figure 8.21 (a), the average propulsive speed vs. consumed power is plotted. The snakelike robot doped with Na^+ can move faster; however, consumed power is large. If it need not move at high speed, we should use the actuators doped with other counterions that can be driven by low power. Figure 8.21(b) shows the average propulsion speed vs. power consumed per distance. If there is no limit to the capacity of a power source, it can be considered that the actuators doped with Na^+ are effective because the robot can move for a short time; however, there is a region of low consumed power achieved only by the robot doped with TEA^+.

From the observation, it can be summarized that if the input voltage is the same, the actuator doped with Na^+ realizes a high-speed swimming motion with high energy consumption, the one doped with TEA^+ can generate slow swimming speed with low energy consumption, and the one doped with Cs^+ has characteristics between those of Na^+ and TEA^+. Note that the actuators can be

adjusted to various characteristics by selecting an appropriate counterion or by mixing several ions in appropriate proportions.

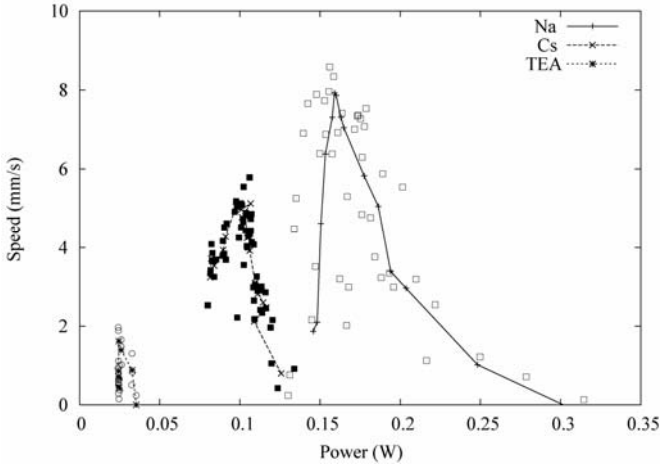

(a)

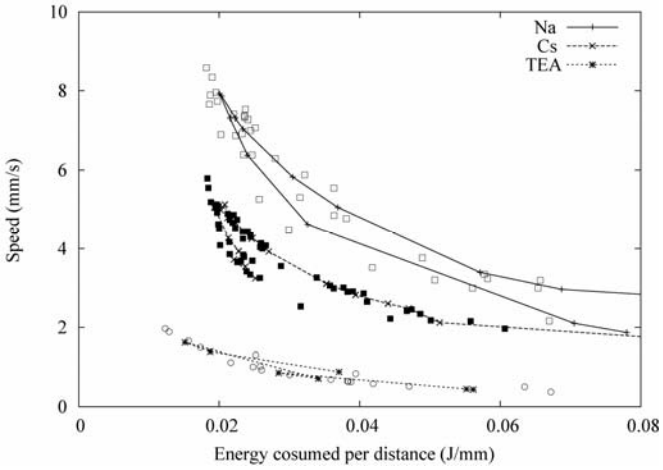

(b)

Figure 8.21. Experimental results of doping effect (a) consumed power vs. average speed (b) consumed energy per distance vs. average speed

8.6 Control of Partial Doping Effect by Exercise

The doping effect is caused by exchanging counterions and a higher condensed counterion is doped into IPMC films. The doping of the counterions is easily done just putting the actuators in a solution containing the target counterion just as the robots take a bath containing a nutritional supplement. When the robots cannot

take a bath, liquid containing the counterion can be delivered to the actuators through tubes like blood vessels. Figure 8.22(a) illustrates these doping processes. If the speed of changing the ion can be controlled by exercises, *i.e.*, bending IPMC films, the property of particular actuators can be changed by such motions. This phenomenon can be considered similar to muscles in a human body that can be trained by exercise for a particular purpose, as in Figure 8.22 (b).

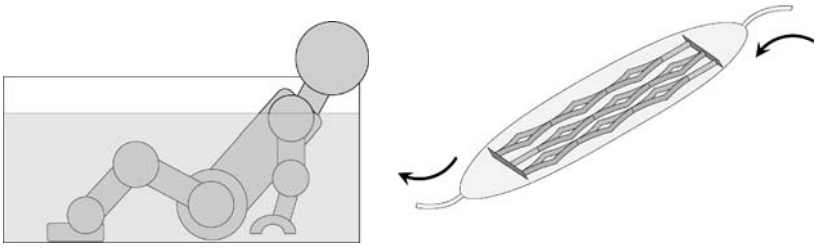

(a)

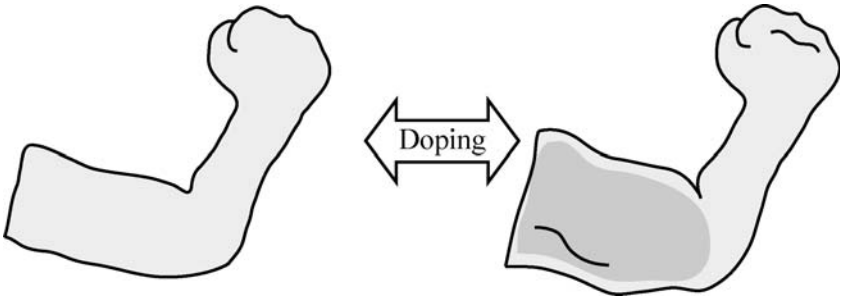

(b)

Figure 8.22. Image of adaptation by doping (a) Process of ion-exchange (b) Adaptation of partial elements by doping

8.6.1 Experiment

To investigate the possibility of the effect in IPMC actuators, we conducted an experiment as follows. Two linear actuators doped with TEA^+ were prepared, and one of the actuators was just immersed in the Na_2SO_4 solution with Na^+. On the other hand, another actuator was actuated in the same solution so that the bending motion was caused frequently.

At every interval, the characteristics of the two actuators were measured. In our experiment, step responses for a constant voltage input are stored.

The length, width, and thickness of the films were 25 mm, 2 mm, and 200 μm, respectively, and they were immersed in the liquid by 15 mm. For the activated film, a rectangular input whose levels were $-1 \leftrightarrow 1$ V and whose frequency was 0.5 s was injected. The step responses of the films were measured at 0, 10, 30, 60, 120, and 180 minutes where the input voltage was 2.0 V.

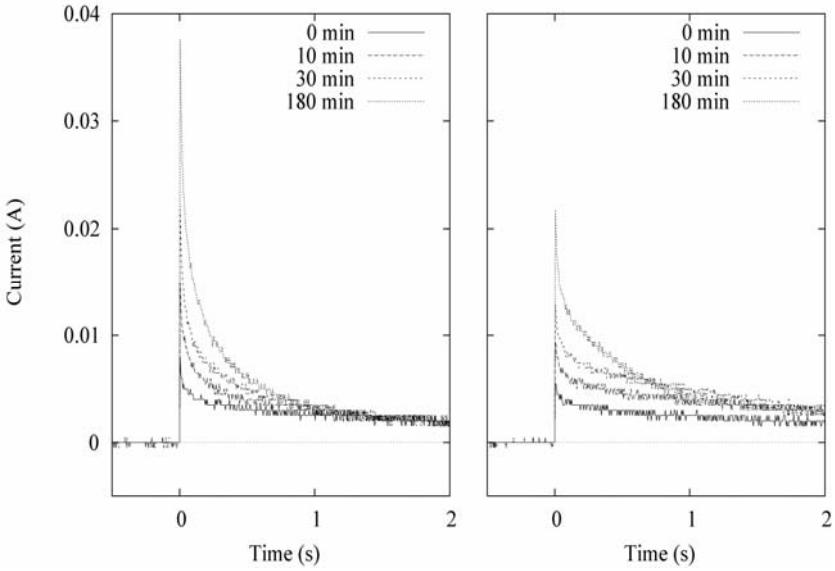

(a)

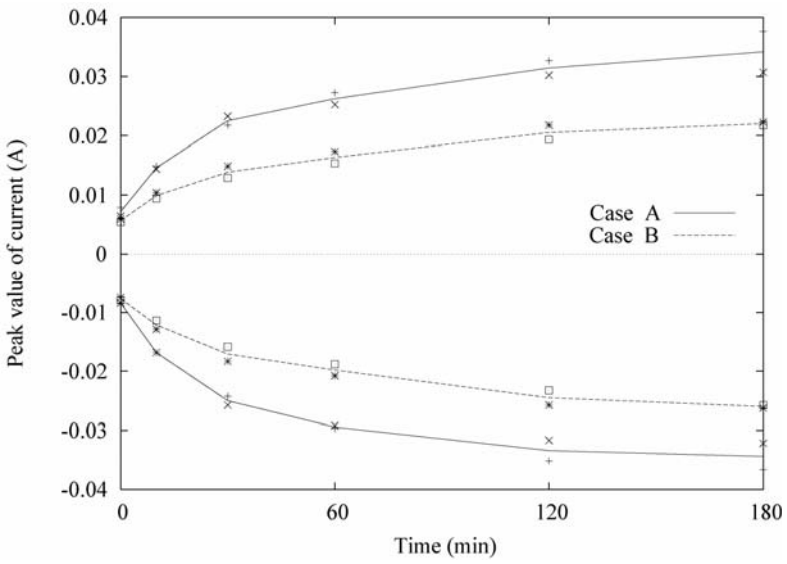

(b)

Figure 8.23. Experimental result of doping progress (a) current (b) peak value of current

When the step response was measured, the actuators were immersed in pure water for 10 minutes to avoid changes due to the mechanical effects of motion.

Figure 8.23 shows the experimental results. In the figure, (a) shows the changes in the current profile for each step input, and (b) shows peak values of the current, with respect to the intervals. From the figure, it can be seen that the peak values of the current increased according to the increase of the interval, and the property was changed from the property of TEA^+ to that of Na^+. Note that the property of the actuator immersed with motion changed more quickly than that without motion. Actually, the property of the film without motion at 180 minutes was achieved by the film with motion at 30 minutes.

8.7 Conclusions

We have discussed the development of a linear actuator using IPMC materials and its applications to a walking robot and a snakelike robot. In this monograph, the doping effects on motion were focused on especially, and it was shown by numerical simulations of walking control and by an experiment of a swimming control of the snakelike robot that the properties of the actuator can be adjusted according to particular motions, *i.e.*, slow speed motion with low energy consumption or high speed motion with high energy consumption. Also, a possibility that some actuators distributed in a system can be partially doped with a desired ion by moving the actuators mechanically was shown by a preliminary experiment. The authors consider that the developed IPMC linear actuator can be used for biomimetic control systems where the properties of the system can be adapted to an environment using doping effects.

To apply the artificial muscle actuator to a general robotic system, there exist a lot of problems such as limitation of output force; however, we think the mutual evolution of improvement of actuator technology and design of control system is important for further applications.

8.8 Acknowledgments

The contents of the paper are collections of works in the last few years by co-workers in the development of the IPMC linear actuator. The authors give their special thanks to Mr. Kaneda, Mr. Kozuki, and Mr. Sera at Tokyo Tech.

8.9 References

Y. Bar-Cohen, Electroactive Polymer (EAP) Actuators as Artificial Muscles: Reality, Potential, and Challenges, SPIE Press, 2001.

K. Oguro, Y. Kawami and H. Takenaka, ``Bending of an ion-conducting polymer film-electrode composite by an electric stimulus at low voltage,'' Journal of Micromachine Society, 5, 27-30, 1992. (in Japanese)

S. Guo, T. Fukuda, K. Kosuge, F. Arai, K. Oguro and M. Negoro, ``Micro catheter system with active guide wire," Proc. of IEEE Int. Conf. on Robotics and Automation, pp.79-84, 1995.

EAMEX Corporation, http://www.eamex.co.jp/

M. Mojarrad and M. Shahinpoor, ``Biomimetic robotic propulsion using polymeric artificial muscles," Proc. of IEEE Int. Conf. on Robotics and Automation, pp.2152-2157, 1997.

S. Guo, T. Fukuda and K. Asaka, ``A new type of fish-like underwater microrobot," IEEE/ASME Trans. on Mechatronics, Vol. 8, No. 1, pp.136-141, 2003.

J. Jung, B. Kim, Y. Tak and J. O. Park, ``Undulatory tadpole robot (TadRob) using ionic polymer metal composite (IPMC) actuator," Proc. of IEEE/RSJ Int. Conf. on Intelligent Robots and Systems, pp.2133-2138, 2003.

J. W. Paquette, K. J. Kim and W. Yim, ``Aquatic robotic propulsor using ionic polymer-metal composite artificial muscle," Proc. of IEEE/RSJ Int. Conf. on Intelligent Robots and Systems, pp.1269-1274, 2004.

A. Punning M. Anton, M. Kruusmaa and A. Aabloo, ``A biologically inspired ray-like underwater robot with electroactive polymer pectoral fins," Proc. of IEEE/ Int. Conf. on Mechatronics and Robotics, Vol. 2, pp.241-245, 2004.

Y. Nakabo, T. Mukai, K. Ogawa, N. Ohnishi and K. Asaka, ``Biomimetic soft robot using artificial muscle," in tutorial ``Electro-Active Polymer for Use in Robotics", IEEE/RSJ Int. Conf. on Intelligent Robots and Systems, 2004.

Y. Bar-Cohen, S. Leary, A. Yavrouian, K. Oguro, S. Tadokoro, J. Harrison, J. Smith and J. Su, ``Challenges to the application of IPMC as actuators of planetary mechanisms," Proc. of SPIE Int. Symp. on Smart Structures and Materials, EAPAD, Vol. 3987, 2000.

S. Guo, S. Hata, K. Sugumoto, T. Fukuda and K. Oguro, ``Development of a new type of capsule micropump," Proc. of IEEE Int. Conf. on Robotics and Automation, pp.2171-2176, 1999.

S. Tadokoro, S. Yamagami, M. Ozawa, T. Kimura and T. Takamori, ``Multi-DOF device for soft micromanipulation consisting of soft gel actuator elements," Proc. of IEEE Int. Conf. on Robotics and Automation, pp.2177-2182, 1999.

S. Tadokoro, S. Fuji, M. Fushimi, R. Kanno, T. Kimura and T. Takamori, ``Development of a distributed actuation device consisting of soft gel actuator elements," Proc. of IEEE Int. Conf. on Robotics and Automation, pp.2155-2160, 1998.

M. Yamakita, N. Kamamichi, Y. Kaneda, K. Asaka and Z. W. Luo, ``Development of an artificial muscle linear actuator using ionic polymer-metal composites," Advanced Robotics, Vol. 18, No. 4, pp.383-399, 2004.

K. Onishi, S. Sewa, K. Asaka, N. Fujiwara and K. Oguro, ``The effects of counter ions on characterization and performance of a solid polymer electrolyte actuator," Electrochemica Acta, Vol. 46, No. 8, pp.1233-1241, 2001.

Y. Kaneda, N. Kamamichi, M. Yamakita, K. Asaka and Z. W. Luo, ``Development of linear artificial muscle actuator using ionic polymer -introduce nonlinear characteristics to attain a higher steady gain-," Proc. of the Annual Conf. of RSJ, 2003. (in Japanese)

S. Tadokoro and T. Takamori, ``Modeling IPMC for design of actuation mechanisms," Electroactive Polymer (EAP) Actuators as Artificial Muscles, Reality, Potential, and Challenges, Ed. Y. Bar-Cohen, SPIE Press, pp.331-366, 2001.

K. Asaka and K. Oguro, ``Bending of polyelectrolyte membrane platinum composites by electric stimuli Part II. Response kinetics," Journal of Electroanalytical Chemistry, 480, pp.186-198, 2000.

S. Tadokoro, S. Yamagami and T. Takamori, ``An actuator model of ICPF for robotic applications on the basis of physicochemical hypotheses," Proc. of IEEE Int. Conf. on Robotics and Automation (ICRA), pp. 1340-1346, 2000.

S. Tadokoro, M. Fukuhara, Y. Maeba, M. Konyo, T. Takamori and K. Oguro, ``A dynamical model of ICPF actuator considering ion-induced lateral strain for molluskan robotics," Proc. of IEEE Int. Conf. on Robotics and Automation, pp. 2010-2017, 2002.

K. Mallavarapu, K. Newbury and D. J. Leo, "Feedback control of the bending response of ionic polymer-metal composite actuators," Proc. of SPIE Int. Symp. on Smart Structures and Materials, EAPAD, Vol. 4329, pp.301-310, 2001.

T. McGeer, ``Passive dynamic walking," The Int. Journal of Robotics Research, Vol. 9, No. 2, pp.62-82, 1990.

M. Yamakita, N. Kamamichi, T. Kozuki, K. Asaka and Z. W. Luo, ``Control of biped walking robot with IPMC linear actuator," Proc. of IEEE/ASME Int. Conf. on Advanced Intelligent Mechatronics, 2005.

M. Yamakita, N. Kamamichi, Y. Kaneda, K. Asaka and Z. W. Luo, ``IPMC linear actuator with re-doping capability and its application to biped walking robot," Proc. of 3rd IFAC Symposium on Mechatronic Systems, pp.359-364, 2004.

M. Yamakita, N. Kamamichi, T. Kozuki, K. Asaka and Z. W. Luo, ``A snake-like swimming robot using IPMC actuator and verification of doping effect," Proc. of IEEE/RSJ Int. Conf. on Intelligent Robots and Systems, 2005.